

Correction and simulation of the intensity compensation algorithm used in curvature wavefront sensing *

Zhi-Xu Wu^{1,2,3}, Hua Bai^{1,2} and Xiang-Qun Cui^{1,2}

¹ National Astronomical Observatories/Nanjing Institute of Astronomical Optics & Technology, Nanjing 210042, China; zxwu@niaot.ac.cn

² Key Laboratory of Astronomical Optics & Technology, Nanjing Institute of Astronomical Optics & Technology, Chinese Academy of Sciences, Nanjing 210042, China

³ University of Chinese Academy of Sciences, Beijing 100049, China

Received 2014 June 24; accepted 2014 September 4

Abstract The wavefront measuring range and recovery precision of a curvature sensor can be improved by an intensity compensation algorithm. However, in a focal system with a fast f-number, especially a telescope with a large field of view, the accuracy of this algorithm cannot meet the requirements. A theoretical analysis of the corrected intensity compensation algorithm in a focal system with a fast f-number is first introduced and afterwards the mathematical equations used in this algorithm are expressed. The corrected result is then verified through simulation. The method used by such a simulation can be described as follows. First, the curvature signal from a focal system with a fast f-number is simulated by Monte Carlo ray tracing; then the wavefront result is calculated by the inner loop of the FFT wavefront recovery algorithm and the outer loop of the intensity compensation algorithm. Upon comparing the intensity compensation algorithm of an ideal system with the corrected intensity compensation algorithm, we reveal that the recovered precision of the curvature sensor can be greatly improved by the corrected intensity compensation algorithm.

Key words: instrumentation — detectors-methods — numerical-techniques — image processing

1 INTRODUCTION

In the imaging process of telescopes, many factors will lead to a decline in image quality, such as optical design, optical fabrication error, gravity deformation and thermal deformation. The theory and implementation of active optics has changed the way telescopes are designed (Su & Cui 1999). Because of active optics, one can make efforts to correct the gravity deformation, temperature deformation, support error and even the mirror machining error (Su & Cui 2004). In active optics, real time sensing of wavefront error is critical. There are two main kinds of wavefront sensors used in active optics: the Shack-Hartmann wavefront sensor and wavefront curvature sensor. The Shack-Hartmann wavefront sensor has been used in many large telescopes, such as the Chinese LAMOST project (Cui et al. 2004; Zhang 2008). The measuring precision achievable with the active optics

* Supported by the National Natural Science Foundation of China.

used in the LAMOST project is extremely high (Stepp 1994). However, in a telescope with a large field of view, the field of view used for sensing is limited by the Shack-Hartmann wavefront sensor, and almost equal to zero. A wavefront curvature sensor is based on the measurement of the wavefront's curvature. Compared with the Shack-Hartmann sensor, it has the advantages of simplicity, high throughput, avoidance of calibration difficulties, etc (Roddier & Roddier 1993). Researchers working with the LSST (Manuel et al. 2010) and VISTA (Patterson & Sutherland 2003) have proposed using this method to measure the wavefront in these large telescopes.

There are two common methods to recover the wavefront by incorporating curvature sensors: the Fast Fourier Transform (FFT) algorithm and the Gerchberg-Saxton algorithm. Both algorithms require that the equivalent defocus distance is small and the wavefront aberration is not very large. Thus, Roddier & Roddier (1993) proposed an intensity compensation algorithm based on an ideal system. By compensating the residual aberration of the defocused images, the wavefront measurement range and recovered precision of the curvature sensor can be greatly improved. Roddier & Roddier used their algorithm in telescopes like the ESO NTT and obtained very good results (Roddier & Roddier 1993), but those tests were applied on a relatively slow Cassegrain focus where distortion errors in the pupil grid could be ignored. In telescopes with a fast f-number, the reference point is very different from that of an ideal system, and distortion errors in the pupil grid will lead to lower recovered precision, thus this algorithm cannot be used in those systems directly. In addition, in the off-axis situation, the angle between the CCD and the defocused surface can also cause coordinate distortion. In this paper, we theoretically deduce the equations for intensity compensation in a telescope with a fast f-number, and simulate the situation on-axis and off-axis in telescopes with a flat image plane. The results show that the corrected intensity performed by the compensation algorithm is better for wavefront recovery in a telescope with a fast f-number.

2 FFT WAVEFRONT RECOVERY ALGORITHM AND INTENSITY COMPENSATION ALGORITHM

Curvature wavefront sensing was first proposed by Roddier (1989), and has successfully been used in adaptive optics. The principle of how a curvature sensor operates is shown in Figure 1. I_1 and I_2 are the defocused images. We can obtain the curvature signal by subtracting I_2 from I_1 and then apply the expression

$$S(r) = \frac{-1 I_2(r) - I_1(r)}{\Delta z I_2(r) + I_1(r)} \approx \nabla^2 W - \delta_c \frac{\partial W}{\partial n}. \quad (1)$$

Here, $\Delta z = \frac{f(f-l)}{l}$, f is the focal length of the optical system, l is the defocus distance, and δ_c is the delta function at the aperture edge. The main task of wavefront recovery is to solve this Poisson

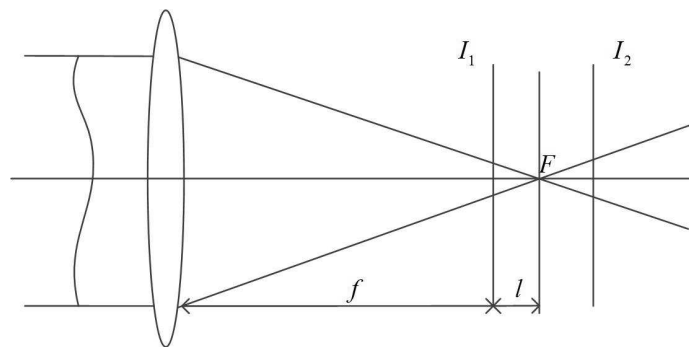


Fig. 1 The principle of how the curvature sensor operates.

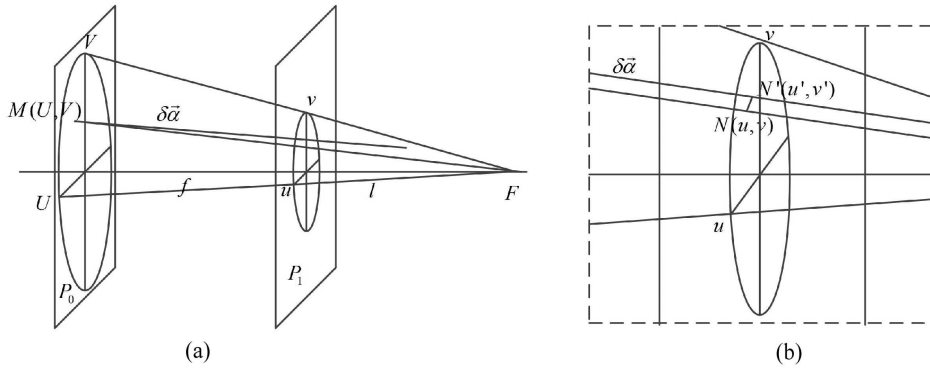


Fig. 2 The principle of how the intensity compensation algorithm operates.

equation with a Neumann boundary condition. If we constrain $\partial W / \partial n$ on the aperture edge, δ_c can be absorbed into Laplacian (Claver et al. 2012)

$$S = \nabla^2 W. \tag{2}$$

We apply a Fourier transform to both sides of Equation (2) yielding

$$FT_{\mu, \nu} \{ \nabla^2 W(x, y) \} = -4\pi^2 (\mu^2 + \nu^2) FT_{\mu, \nu} \{ W(x, y) \}. \tag{3}$$

Thus

$$W = IFT_{x, y} \left\{ \frac{FT_{\mu, \nu}(S)}{-4\pi^2 (\mu^2 + \nu^2)} \right\}. \tag{4}$$

The method mentioned above is only a first order approximation, valid for small Δz , i.e. highly defocused images. The solution of the FFT algorithm should be used as a first order solution. Roddier discovered that the intensity compensation algorithm, which compensates the residual aberration of the defocused images, can improve the precision of wavefront recovery (Roddier & Roddier 1993). As shown in Figure 2, R is the radius of the telescope’s pupil and the normalized coordinate of the pupil is $x = U/R, y = V/R$. The normalized coordinate in the defocused surface is $x' = uf/lR, y' = vf/lR$.

Assuming no aberration, the ray from M will converge toward F and cross the defocused surface at point N . Because of the aberration $W(x, y)$, the ray from M will converge to N' . The coordinate of N' is given by

$$\begin{cases} x' = x + C\partial W(x, y)/\partial x \\ y' = y + C\partial W(x, y)/\partial y \end{cases}, \tag{5}$$

with $C = -\frac{f(f-l)}{l} \frac{1}{R^2}$. To compensate the intensity of N' to N , the expression should be

$$I(x, y) = I'(x', y') \left\{ 1 + C \left(\frac{\partial^2 W}{\partial x^2} + \frac{\partial^2 W}{\partial y^2} \right) + C^2 \left[\frac{\partial^2 W}{\partial x^2} \frac{\partial^2 W}{\partial y^2} - \left(\frac{\partial^2 W}{\partial xy} \right)^2 \right] \right\}. \tag{6}$$

3 THE CORRECTED INTENSITY COMPENSATION ALGORITHM

3.1 The Correction in a Telescope with a Fast f-number

In telescopes with a fast f-number, the wavefront of the exit pupil in an unaberrated system is spherically centered at the focal point of the image. As shown in Figure 3(a), the ray tracing of this spherical wavefront is equivalent to the ideal surface S ; the diameter of S is obviously larger than the exit

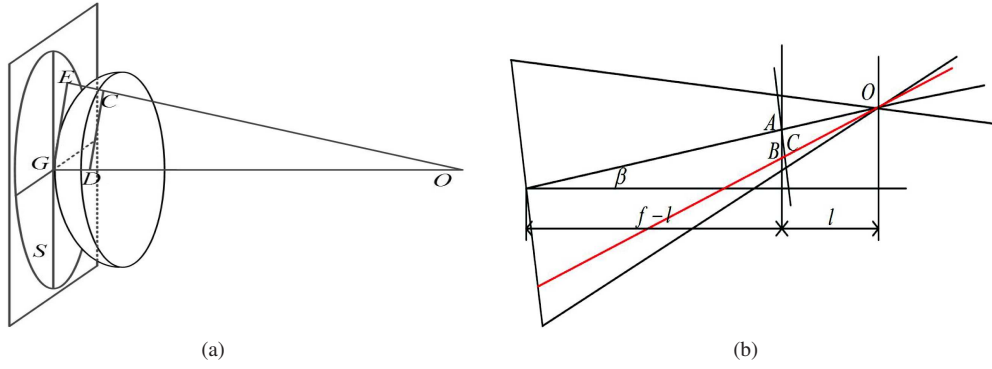


Fig. 3 (a) The correction of the on-axis coordinates; (b) The correction of the off-axis coordinates.

pupil, thus the defocused image is different from that generated in an ideal system. Furthermore, the FFT algorithm must take into consideration the edge information $\delta_c \frac{\partial W}{\partial n}$ of the curvature signal. The projection of the equivalent surface S will cause the curvature signal to stretch beyond the bounds of the pupil edge; that information will be masked off by the pupil. Therefore, the coordinates relative to the spherical wavefront need to be corrected to the coordinates relative to the surface S . The equations describing this correction is

$$\begin{cases} x' = D_1(x, y) \cdot x + C \partial W(x, y) / \partial x \\ y' = D_2(x, y) \cdot y + C \partial W(x, y) / \partial y \end{cases} \quad (7)$$

where $D_1(x, y)$ and $D_2(x, y)$ are the coordinate correction factors, which are equal to 1 for the paraxial case and C is constant. Because $\frac{GE}{DC} = \frac{GO}{DO}$ and

$$GO = f, \quad DO = \sqrt{CO^2 - DC^2} = \sqrt{f^2 - (x^2 + y^2) \cdot R^2},$$

thus

$$GE = \frac{f \cdot R}{\sqrt{f^2 - (x^2 + y^2) \cdot R^2}} \cdot \sqrt{(x^2 + y^2)}. \quad (8)$$

The component of GE on the x -axis is

$$X = \frac{1}{R} \cdot GE \cdot \cos \theta = \frac{1}{R} GE \cdot \frac{x}{\sqrt{(x^2 + y^2)}} = \frac{f}{\sqrt{f^2 - (x^2 + y^2) \cdot R^2}} \cdot x. \quad (9)$$

Thus the correction factor on the x -axis is

$$D_1(x, y) = \frac{f}{\sqrt{f^2 - (x^2 + y^2) \cdot R^2}}. \quad (10)$$

Similarly, we can derive the correction factor for the y -axis to be

$$D_2(x, y) = \frac{f}{\sqrt{f^2 - (x^2 + y^2) \cdot R^2}}. \quad (11)$$

In the off-axis case, as shown in Figure 3(b), the CCD is perpendicular to the optical axis, resulting in an angle between the CCD and the curvature signal from the surface. Firstly we must compensate

the coordinate distortion induced by this angle, and then use the equation for the on-axis case to compensate the coordinates. Assuming the field of view is (α, β) , in the meridional plane we have

$$\frac{AB}{AC} = \frac{\sin \angle ACB}{\sin \angle ABC} = \frac{\sin \angle ACB}{\sin(180^\circ - \angle ACB - \beta)}. \quad (12)$$

Since $\tan \angle AOC = \frac{y \cdot R}{f / \cos \beta}$, then

$$AC = \frac{AB}{\cos \beta - \sin \beta \cdot \cos \beta \frac{y \cdot R}{f}}. \quad (13)$$

Similarly, we can obtain the coordinate compensation equation in the sagittal plane

$$AC = \frac{AB}{\cos \alpha - \sin \alpha \cdot \cos \alpha \frac{y \cdot R}{f}}. \quad (14)$$

3.2 Comparing the Coordinates Before and After Correction

Compensation for the distortion of the coordinate on the axis is a procedure that involves nonlinear scaling. As shown in Figure 4(a) and Figure 4(b), the correction factor is the smallest in the center of the aperture and the scale of the ratio is 1. In the off-axis case, we can see from Figure 4(c) and Figure 4(d) that aside from the nonlinear scaling of the coordinate, there is also a tilt factor that is applied to the coordinate.

4 RESULTS OF THE SIMULATION

In order to test the intensity compensation algorithm, we adopt the optical system of a Schmidt telescope with a flat image plane as the simulation system (as show in Fig. 5). The system parameters we used are $f = 100$ mm, aperture diameter $D = 75$ mm, defocus length $l = 1$ mm, wavelength $\lambda = 550$ nm, and the fields of view used for simulation are $(0^\circ, 0^\circ)$ and $(0^\circ, 0.5^\circ)$.

Even though the ray tracing ignored the effect of diffraction from the edge of the aperture, the curvature signal simulated by ray tracing has sufficient accuracy to recover the wavefront. The size of the CCD that we simulate at the defocused surface is 1 mm, and the pixels are arranged in a 200×200 grid. The entry pupil is sampled by the Monte Carlo method and performs a ray trace for each sample point. We can simulate the defocused images by tracing 10^5 rays.

The wavefront recovery process is shown in Figure 6: First, we simulate the defocused images by Monte Carlo ray tracing and compensate the off-axis coordinate distortion. Second, we create the curvature signal to recover the raw wavefront by the FFT wavefront recovery algorithm. Third, by inputting the raw wavefront to the corrected intensity compensation algorithm, we obtain the compensated defocused images. Fourth, we estimate the wavefront by the FFT algorithm and repeat these steps until the accuracy of the estimated wavefront meets the requirements. In order to prevent oscillations caused by intensity compensation, a compensating factor needs to be multiplied (in this paper, the compensating factor is 0.6). Furthermore, we compensate the high order aberrations after compensating the lower order aberrations and the maximum order is 22.

Variation in the curvature signal for the on-axis situation is shown in Figure 7. Z4 is being compensated in the first iteration. Z4–Z6 of the Zernike coefficients are being compensated from the second to the fifth iterations. Z4–Z13 of the Zernike coefficients are being compensated from the eighth to the twelfth iterations. Z4–Z22 of the Zernike coefficients are being compensated from the twelfth to the twentieth iterations. We can see from the last result that the curvature information from the curvature signal is almost zero, and the information about the aperture edge is also zero.

The on-axis and off-axis wavefront is shown in Figure 8. The on-axis aberration parameters are: the PV value is 6.653λ and the RMS is 1.137λ ; the off-axis aberration parameters are: the PV value

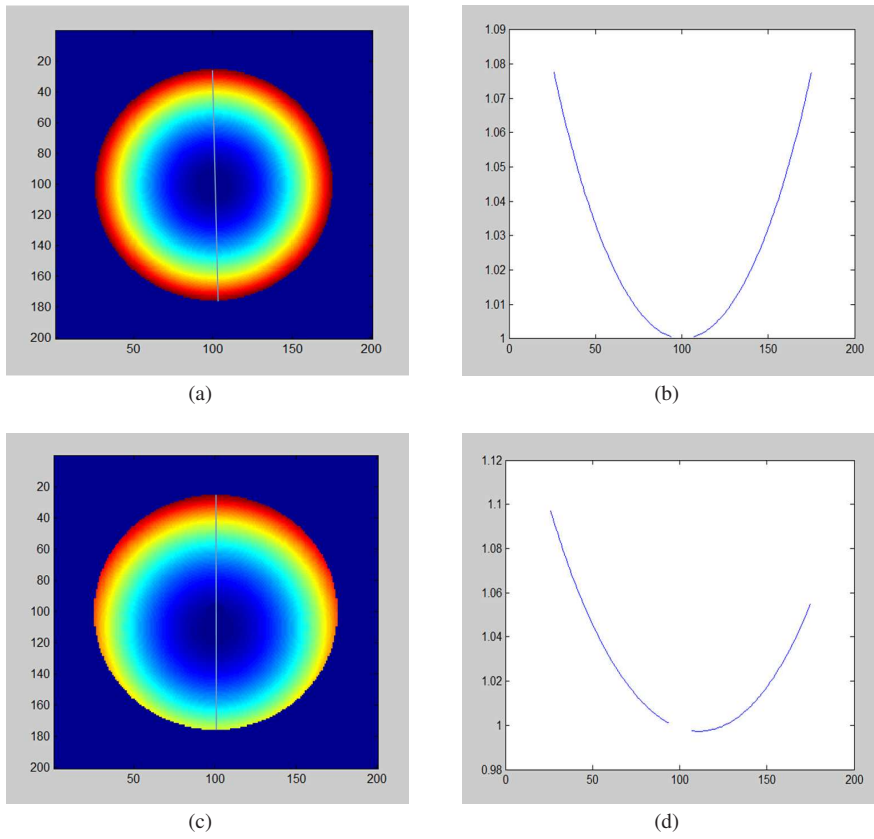


Fig. 4 (a) Correction factor for on-axis coordinates; (b) vertical examples of the correction factor; (c) correction factor for off-axis coordinates; (d) vertical examples of the correction factor.

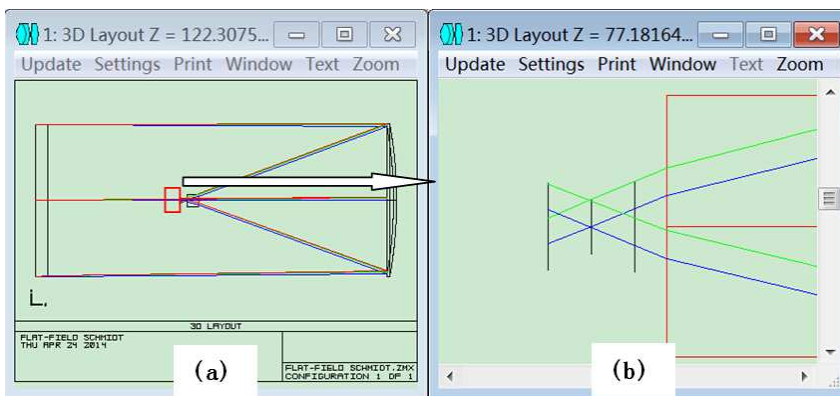


Fig. 5 (a) Schmidt telescope with a flat image plane; (b) the defocused surface.

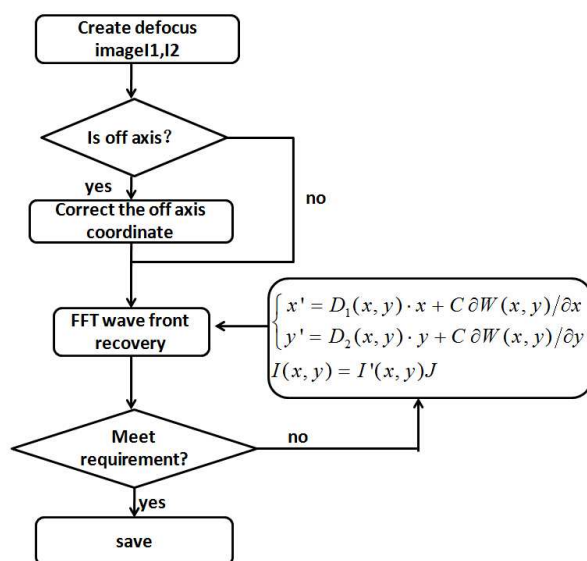


Fig. 6 A flow chart of the wavefront recovery algorithm.

is 6.663λ and the RMS is 1.14λ ($\lambda = 550$ nm). The coefficients of the wavefront Zernike terms are shown in the first row of Tables 1 and 2. Because of vignetting, information about the top of the off-axis wavefront is lost. Although the vignetting will introduce fitting errors in the Zernike coefficients, the errors are too small to effect the accuracy of wavefront recovery.

The results of the simulation are shown in Tables 1 and 2. The third row in the tables is the Zernike coefficients recovered by the FFT wavefront recovery algorithm. For large aberrations (about 1 wavelength), the RMS of the recovered on-axis wavefront is 114 nm, and the RMS of the recovered off-axis wavefront is 128 nm. The results do not meet the requirements of wavefront sensing. The results shown in the fourth row are the Zernike coefficients recovered by the FFT wavefront recovery algorithm with the ideal intensity compensation algorithm. Even though more curvature signals are used in the FFT wavefront recovery algorithm, the accuracy still cannot meet the requirements because of coordinate distortion. The last rows in Tables 1 and 2 are the results recovered by the inner iteration of the FFT algorithm and the outer iteration of the corrected intensity compensation algorithm. The accuracy is highly improved because the distortion in the coordinate is removed by the coordinate correction. The on-axis RMS declines from 52.9 nm to 12.4 nm, and the off-axis RMS declines from 82.5 nm to 13.7 nm. The simulation results indicate that the corrected intensity compensation algorithm is more reasonable for wavefront recovery in a telescope with a fast f-number.

Table 1 The Result of On-axis Wavefront Recovery

Zernike Terms	Z4	Z5	Z6	Z7	Z8	Z9	Z10	Z11	Z12	
Zernike Coefficients (λ)	-0.720	-0.602	0	0	0.502	0	-0.401	-0.017	0	RMS (nm)
FFT	-0.591	-0.651	-0.013	0.025	0.528	0.023	-0.243	0.006	-0.011	114
Paraxial	-0.797	-0.628	-0.025	0	0.495	0.009	-0.413	-0.022	-0.005	52.9
On-axis	-0.725	-0.609	0.018	0.013	0.500	0.008	-0.403	-0.018	0	12.4

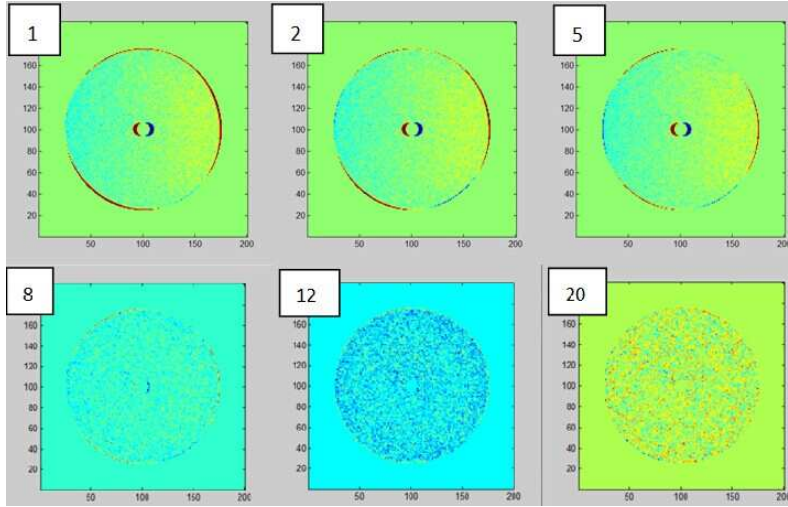


Fig. 7 The changes in the curvature signal during the compensation. The numbers in the upper left corner are the iteration numbers.

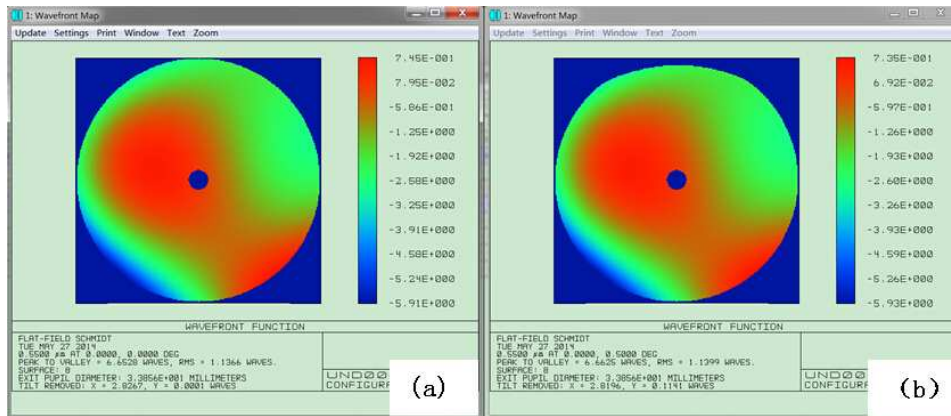


Fig. 8 (a) The on-axis wavefront; (b) the off-axis wavefront.

Table 2 The Result of Off-axis Wavefront Recovery

Zernike Terms	Z4	Z5	Z6	Z7	Z8	Z9	Z10	Z11	Z12	
Zernike Coefficients (λ)	-0.729	-0.602	0.004	0.013	0.502	0	-0.401	-0.017	0	RMS (nm)
FFT	-0.533	-0.662	0.032	0.018	0.512	0.018	-0.427	0.001	-0.002	128
Paraxial	-0.654	-0.633	-0.030	0.032	0.390	0	-0.430	-0.028	0.014	82.5
Off-axis	-0.727	-0.614	0.023	0.017	0.488	0.008	-0.399	-0.016	0	13.7

5 CONCLUSIONS

In this paper, we analyze the corrected intensity compensation algorithm of a focal system with a fast f-number and apply this algorithm to recover the wavefront of a Schmidt telescope with a flat

image plane. By comparing simulation results of the ideal intensity compensation algorithm with the corrected intensity compensation algorithm, we confirm that the corrected intensity compensation algorithm is more reasonable for a focal system with a fast f-number.

Acknowledgements This work was supported by the National Natural Science Foundation of China (Grant Nos. 11103048, 11190013 and 11273038).

References

- Claver, C. F., Chandrasekharan, S., Liang, M., et al. 2012, in Society of Photo-Optical Instrumentation Engineers (SPIE) Conference Series, 8444, 14
- Cui, X., Su, D., Li, G., et al. 2004, in Society of Photo-Optical Instrumentation Engineers (SPIE) Conference Series, 5489, Ground-based Telescopes, ed. J. M. Oschmann, Jr., 974
- Manuel, A. M., Phillion, D. W., Olivier, S. S., Baker, K. L., & Cannon, B. 2010, Optics Express, 18, 1528
- Patterson, B. A., & Sutherland, W. J. 2003, in Society of Photo-Optical Instrumentation Engineers (SPIE) Conference Series, 4842, Specialized Optical Developments in Astronomy, eds. E. Atad-Ettdgui, & S. D'Odorico, 231
- Roddier, C., & Roddier, F. 1993, Journal of the Optical Society of America A, 10, 2277
- Roddier, N. 1989, Curvature Sensing for Adaptive Optics: A Computer Simulation, Master's Thesis, The University of Arizona
- Stepp, L. M., ed. 1994, Society of Photo-Optical Instrumentation Engineers (SPIE) Conference Series, 2199, Advanced Technology Optical Telescopes V
- Su, D., & Cui, X. 1999, Progress in Astronomy, 17, 1
- Su, D.-Q., & Cui, X.-Q. 2004, ChJAA (Chin. J. Astron. Astrophys.), 4, 1
- Zhang, Y. 2008, in Society of Photo-Optical Instrumentation Engineers (SPIE) Conference Series, 7012, 70123H-11